Optical Images of an Exosolar Planet 25 Light-Years from Earth

Paul Kalas, *et al.*

Science **322**, 1345 (2008);
DOI: 10.1126/science.1166609

Science (print ISSN 0036-8075; online ISSN 1095-9203) is published weekly, except the last week in December, by the American Association for the Advancement of Science, 1200 New York Avenue NW, Washington, DC 20005.

Optical Images of an Exosolar Planet 25 Light-Years from Earth

Paul Kalas,[1]* James R. Graham,[1] Eugene Chiang,[1,2] Michael P. Fitzgerald,[3] Mark Clampin,[4] Edwin S. Kite,[2] Karl Stapelfeldt,[5] Christian Marois,[6] John Krist[5]

Fomalhaut, a bright star 7.7 parsecs (25 light-years) from Earth, harbors a belt of cold dust with a structure consistent with gravitational sculpting by an orbiting planet. Here, we present optical observations of an exoplanet candidate, Fomalhaut b. Fomalhaut b lies about 119 astronomical units (AU) from the star and 18 AU of the dust belt, matching predictions of its location. Hubble Space Telescope observations separated by 1.73 years reveal counterclockwise orbital motion. Dynamical models of the interaction between the planet and the belt indicate that the planet's mass is at most three times that of Jupiter; a higher mass would lead to gravitational disruption of the belt, matching predictions of its location. The flux detected at 0.8 μm is also consistent with that of a planet with mass no greater than a few times that of Jupiter. The brightness at 0.6 μm and the lack of detection at longer wavelengths suggest that the detected flux may include starlight reflected off a circumplanetary disk, with dimension comparable to the orbits of the Galilean satellites. We also observe variability of unknown origin at 0.6 μm.

About 15% of nearby stars are surrounded by smaller bodies that produce copious amounts of fine dust via collisional erosion (*1*). These "dusty debris disks" are analogs to our Kuiper Belt and can be imaged directly through the starlight they reflect or thermal emission from their dust grains. Debris disks may be gravitationally sculpted by more massive objects; their structure gives indirect evidence for the existence of accompanying planets [e.g., (*2*, *3*)]. Fomalhaut, an A3V star 7.69 pc from the Sun (*4*), is an excellent example: A planet can explain the observed 15 AU offset between the star and the geometric center of the belt, as well as the sharp truncation of the belt's inner edge (*3*, *5*–*7*). With an estimated age of 100 to 300 million years (My) (*8*), any planet around Fomalhaut would still be radiating its formation heat and would be amenable to direct detection. The main observational challenge is that Fomalhaut is one of the brightest stars in the sky (apparent visual magnitude m_V = 1.2 mag); to detect a planet around it requires the use of specialized techniques such as coronagraphy to artificially eclipse the star and suppress scattered and diffracted light.

Detection of Fomalhaut b. Coronagraphic observations with the Hubble Space Telescope (HST) in 2004 produced the first optical image of Fomalhaut's dust belt and detected several faint sources near Fomalhaut (*6*). Fomalhaut's proper motion across the sky is 0.425 arc sec per year in the southeast direction, which means that objects that are in the background will appear to move northwest relative to the star. To find common proper motion candidate sources, we observed Fomalhaut with the Keck II 10-m telescope in 2005 and with HST in 2006 (*9*). In May 2008, a comprehensive data analysis revealed that Fomalhaut b is physically associated with the star and displays orbital motion. Follow-up observations were then conducted at Gemini Observatory at 3.8 μm (*9*).

Fomalhaut b was confirmed as a real astrophysical object in six independent HST observations at two optical wavelengths (0.6 μm and 0.8 μm; Fig. 1 and table S1). It is comoving with Fomalhaut, except for a 0.184 ± 0.022 arc sec (1.41 ± 0.17 AU) offset between 2004 and 2006 (ΔT = 1.73 years) corresponding to 0.82 ± 0.10 AU year^{-1} projected motion relative to Fomalhaut (*9*). If Fomalhaut b has an orbit that is coplanar and nested within the dust belt, then its semimajor axis is $a \approx 115$ AU, close to that predicted by Quillen (*7*). An object with a = 115 AU in near-circular Keplerian motion around a star with mass 2.0 times that of the Sun has an orbital period of 872 years and a circular speed of 3.9 km s^{-1}. The six Keplerian orbital elements are unconstrained by measurements at only two epochs; however, by comparing the deprojected space velocity ($5.5^{+1.1}_{-0.7}$ km s^{-1}) with the circular speed, we

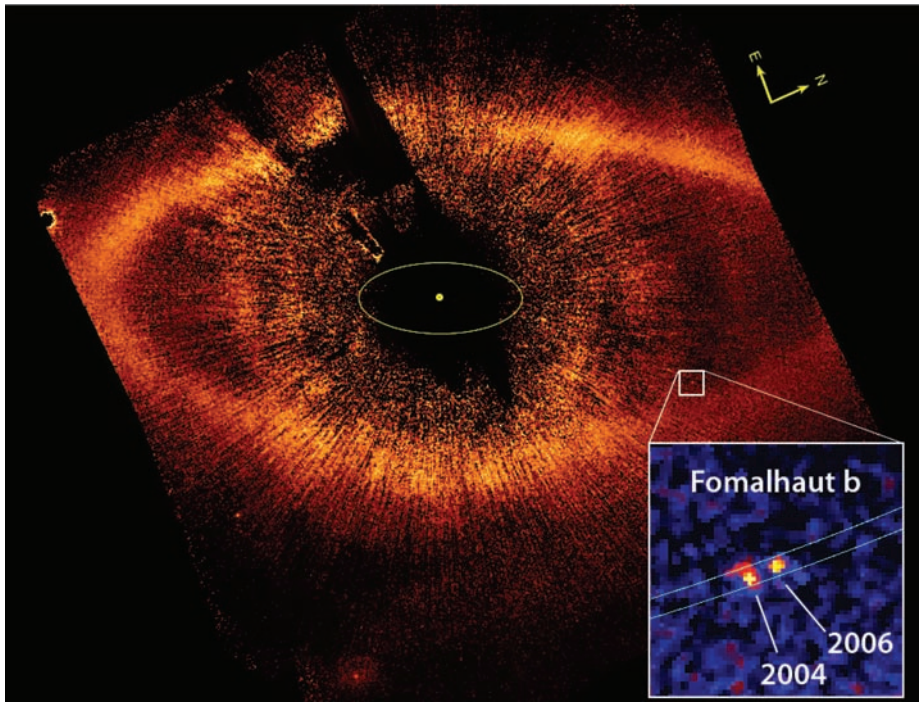

Fig. 1. HST coronagraphic image of Fomalhaut at 0.6 μm, showing the location of Fomalhaut b (white square) 12.7 arc sec radius from the star and just within the inner boundary of the dust belt. All the other apparent objects in the field are either background stars and galaxies or false positives. The fainter lower half of the dust belt lies behind the sky plane. To obtain an orientation with north up and east left, this figure should be rotated 66.0° counterclockwise. The yellow circle marks the location of the star behind the occulting spot. The yellow ellipse has a semimajor axis of 30 AU at Fomalhaut (3.9 arc sec) that corresponds to the orbit of Neptune in our solar system. The inset is a composite image showing the location of Fomalhaut b in 2004 and 2006 relative to Fomalhaut. Bounding Fomalhaut b are two elliptical annuli that are identical to those shown for Fomalhaut's dust belt (*6*), except that here the inner and outer annuli have semimajor axes of 114.2 and 115.9 AU, respectively. The motion of Fomalhaut b therefore appears to be nested within the dust belt.

[1]Astronomy Department, University of California, Berkeley, CA 94720, USA. [2]Department of Earth and Planetary Science, University of California, Berkeley, CA 94720, USA. [3]Institute of Geophysics and Planetary Science, Lawrence Livermore National Laboratory, Livermore, CA 94551, USA. [4]Exoplanets and Stellar Astrophysics Laboratory, Goddard Space Flight Center, Greenbelt, MD 20771, USA. [5]MS 183-900, Jet Propulsion Laboratory, California Institute of Technology, Pasadena, CA 91109, USA. [6]Herzberg Institute for Astrophysics, Victoria, British Columbia V9E 2E7, Canada.

*To whom correspondence should be addressed. E-mail: kalas@astron.berkeley.edu

find a lower limit on the eccentricity of 0.13 (95% confidence) by assuming that Fomalhaut b is at periastron. Thus, our observations are consistent with bound Keplerian motion, although the exact range of allowable eccentricity depends sensitively on poorly known uncertainties in orbital inclination, apsidal orientation, and host stellar mass.

Fomalhaut b is located near the faint half of the belt seen in stellar light backscattered by dust grains. Therefore, it lies behind the sky plane (the Earth–Fomalhaut–Fomalhaut b angle is 126°), at ~51° past conjunction as it orbits counterclockwise. Although faint, Fomalhaut b is still 100 times as bright as reflected light from a Jupiter-like planet at that radius from Fomalhaut (*9*).

Dynamical models of planet-belt interaction. We constrained the mass of Fomalhaut b by modeling its gravitational influence on the dust belt, reproducing properties of the belt inferred from the HST scattered-light images. Our model assumes that Fomalhaut b is solely responsible for the observed belt morphology. This assumption implies that the orbits of the belt and of Fomalhaut b are apsidally aligned. The deprojected space velocity and current location of Fomalhaut b are nominally inconsistent with this expectation. Apsidal misalignment may imply the existence of additional perturbers; then the mass estimates derived from our single-planet models are upper limits.

Our modeling procedure comprises four steps. First, for a given mass and orbit of Fomalhaut b, we create a population of several thousand parent bodies stable to gravitational perturbations from the planet. These parent bodies, modeled as test particles, do not undergo close encounters with Fomalhaut b over a 100-My period. Initial parent body orbits have semimajor axes between 120 and 140 AU, and their eccentricities and longitudes of periastron are purely secularly forced by the planet (*10*). Initial inclinations of parent bodies are randomly and uniformly distributed within 0.025 rad of Fomalhaut b's orbital plane, and remaining orbital angles are drawn at random. After 100 My, parent body orbits differ somewhat from these initial conditions; most survivors have semimajor axes of >130 AU. The forced orbits thus constructed are nested ellipses with eccentricity of ~0.11 that approximate the observed belt morphology. Forced orbits are expected to result from interparticle collisions, which dissipate random motions and compel planetesimals to conform toward closed, nonintersecting paths (*11*).

This elliptical annulus of parent bodies is termed a "birth ring" (*12*); erosive collisions among parent bodies give birth to smaller but more numerous dust grains. The observed scattered stellar light predominantly arises not from parent bodies but rather from their dust progeny. Thus, the second step of our procedure is to track dust trajectories. We take each parent to release a dust grain with the same instantaneous position and velocity as its parent's. The trajectory of a grain of given β (force of radiation pressure relative to that of stellar gravity; β scales inversely as grain radius) is then integrated forward under the effects of radiation pressure and Poynting-Robertson drag. We carry out integrations for $\beta \in (0, 0.00625, 0.0125, \ldots, 0.4)$. For β approaching the radiation blowout value of ~½, grains execute highly elongated orbits whose periastra are rooted within the birth ring. Integrations last 0.1 My, corresponding to the collisional lifetime of grains in Fomalhaut's belt, as estimated from the inferred optical depth of the belt.

Third, we superpose the various β integrations to construct maps of optical depth normal to the belt plane. To reduce the shot noise associated with a finite number of grains, we smear each grain along its orbit: Each grain is replaced by an elliptical wire whose linear density along any segment is proportional to the time that a particle in Keplerian motion spends traversing that segment. We compute the optical depth presented by the collection of wires, weighting each β integration according to a Dohnanyi (*13*) grain size distribution. This distribution, which reflects a quasi-steady collisional cascade in which parent bodies grind down to grains so small they are expelled by radiation pressure, is assumed to hold in the birth ring, where dust densities are greatest and collision rates are highest.

The final step is to compare the optical depth profile of our dynamical model with that of a scattered-light model adjusted to fit the 2004 HST image of Fomalhaut's belt (*6*). We focus on the one belt property that seems most diagnostic of planet mass and orbit: the belt's inner edge, having a semimajor axis of $a_{\mathrm{inner}} = 133$ AU according to the scattered-light model. This edge marks the outer boundary of the planet's chaotic zone (*7*). The chaotic zone is a swath of space, enclosing the planet's orbit, that is purged of material because of dynamical instabilities caused by overlapping first-order mean-motion resonances (*14*). For a given planet mass M, we adjust the planet's semimajor axis a until the dynamical model's optical depth attains half its maximum value at a_{inner} (Fig. 2, bottom). Applying this procedure, we find that

$$a_{\mathrm{inner}} - a = 2.0(M/M_*)^{2/7}a \qquad (1)$$

where M_* is the central stellar mass.

Two trends that emerge from our modeling imply that the mass of the planet should be low. First, as M increases, the planet more readily perturbs dust grains onto eccentric orbits, and the resultant optical depth profile becomes too

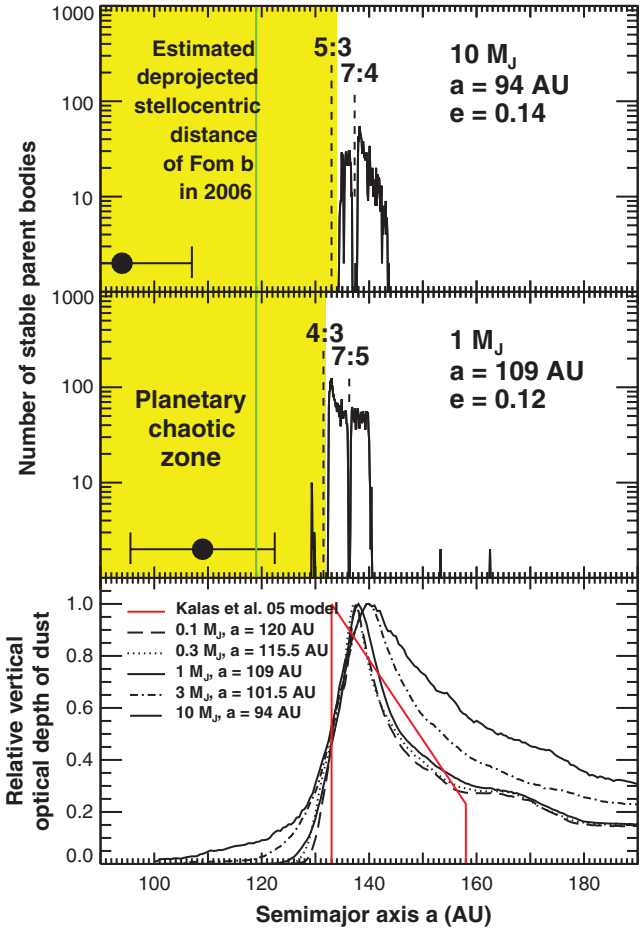

Fig. 2. Dynamical models of how Fomalhaut b gravitationally sculpts the belt [see also (*15*)]. (**Top** and **middle**) Histograms of time-averaged semimajor axes of parent bodies that survive 100-My integrations with Fomalhaut b, whose parameters are chosen to reproduce the belt's inner edge at 133 AU and ellipticity of 0.11. Parent bodies are evacuated from Fomalhaut b's chaotic zone (yellow region). Gaps open at the planet's resonances, akin to the solar system's Kirkwood gaps. Black circles and bars mark the range of stellocentric distances spanned by the model orbits for Fomalhaut b. The apocentric distance for 10 M_J is inconsistent with the observed stellocentric distance of Fomalhaut b (green line). The 1-M_J model is consistent. (**Bottom**) Vertical optical depth profiles of dust generated from parent bodies. The planet orbit is tuned so that the optical depth is at half maximum at 133 AU, the location of the inner edge of the scattered-light model from (*6*) (red curve), which itself is an idealized and non-unique fit to the HST data. Although the dynamical and scattered-light models do not agree perfectly, lower planet masses are still inferred because they do not produce broad tails of emission at $a >$ ~140 AU. At $a >$ ~160 AU, the HST data are too uncertain to constrain any model.

broad at distances greater than ~140 AU (Fig. 2, bottom). Second, for the belt to remain undisrupted, larger-mass planets must have smaller orbits, violating our estimate for the current stellocentric distance of Fomalhaut b (Fig. 2, top and middle). Together, these considerations imply that $M < 3$ Jupiter masses (M_J). This upper limit supersedes those derived previously (*7*), as the quantitative details of our model are more realistic [see also (*15*)]: The belt as a whole is modeled, not just its inner edge; parent bodies are handled separately from dust grains, and only the latter are used to compare with observations; stellar radiation pressure is accounted for; parent bodies are screened for dynamical stability over the system age; and grain-grain collisions are recognized as destructive, so that dust particle integrations are halted after a collision time.

Model planet atmospheres. Comparison between our photometric data and planet atmosphere model–derived spectra indicate that Fomalhaut b may be a cooling jovian-mass exoplanet with an age of 100 to 300 My (Fig. 3). A planet atmosphere model with effective temperature T_{eff} = 400 K and radius 1.2 R_J, for which the bolometric luminosity is 3.4×10^{-7} times that of the Sun ($L_\odot$) (*16*, *17*), reproduces the observed 0.8-μm flux. This model implies that the luminosity of Fomalhaut b is lower than that of any other object observed outside the solar system, and thus that it is not a young brown dwarf or a more massive object. Theoretical cooling tracks of objects with T_{eff} = 400 K and ages of >100 My are insensitive to uncertain initial conditions [see figure 1 of (*16*)]. The luminosity on these tracks is given by $L \sim 2 \times 10^{-7}\,[M/(2\,M_J)]^{1.87}\,(t/200\text{ My})^{-1.21}\,L_\odot$, implying that the mass of Fomalhaut b is 1.7 to 3.5 M_J. The error in the mass is dominated by the age uncertainty.

Relative to the planet atmosphere models, the flux of Fomalhaut b is too faint by at least a factor of 3 at 1.6 μm, and the upper limit set by observations at 3.8 μm is only marginally consistent with the models. However, the various models disagree with each other by similar factors at 1.6 μm, partly because of theoretical uncertainties associated with the strengths of the CH_4 vibrational bands. Moreover, our hypothesized effective temperature is near the condensation temperature of water clouds, and such clouds are a large source of uncertainty in planet atmosphere models. Nonetheless, our observations at 1.6 μm and 3.8 μm exclude a warmer (more massive) planet.

Choosing a 400 K, 46 m s^{-2}, 5× solar abundance model from (*16*) as a baseline, we can investigate the effects of gravity and composition with the use of theoretical exoplanet model spectra (*16*, *17*). The elevated abundance set is chosen to be representative of solar system gas giants. The temperature and gravity of this model are a good match to a 2.5 M_J exoplanet with an age of 200 My. As previously noted, this model accounts for the 0.8-μm flux but overpredicts the 1.6-μm band flux by a factor of 3. Cooler models (350 K) cannot simultaneously reproduce the 0.8-μm flux without violating the long-wavelength flux limits, whereas for hotter models (500 K) the 1.6-μm upper limit becomes particularly problematic. If there is a significant thermal photospheric contribution to the 0.8-μm flux, then 400 K is a rough upper limit to the temperature of the object.

The 400 K solar abundance model has reduced methane opacity, which causes it to be unacceptably bright in the H band. The colors and fluxes also depend on the surface gravity. Models from (*16*) for 10 m s^{-2} and 215 m s^{-2} are also available; the colors of the low-gravity model are too red in both the 0.8- to 1.6-μm and 0.8- to 3.8-μm ranges to be acceptable. Thus, if the gravity is lower than our nominal assumption, corresponding to a ~0.5 M_J object, then we estimate that the upper limit on temperature is raised by about 50 K. The colors of the high-gravity 400 K model are similar to those of the 46 m s^{-2} one.

Other sources of optical emission. From 0.6 to 0.8 μm, Fomalhaut b is bluer than the models predict (Fig. 3). Furthermore, between 2004 and 2006 Fomalhaut b became fainter by ~0.5 mag at 0.6 μm. Photometric variability and excess optical emission cannot be explained by exoplanet thermal radiation alone. The 0.6-μm flux might be contaminated by Hα emission (*9*) that is detected from brown dwarfs (*18*, *19*). Variable Hα emission might arise from a hot planetary chromosphere heated by vigorous internal convection, or trace hot gas at the inner boundary of a circumplanetary accretion disk, by analogy with magnetospheric emission from accreting T Tauri stars [e.g., (*20*)]. If a circumplanetary disk is extended, the starlight it reflects might contribute to the flux detected at 0.6 and 0.8 μm. To explain our observed fluxes requires a disk radius of ~20 to 40 R_J, comparable to the orbital radii of Jupiter's Galilean satellites (*9*). The need for additional sources of luminosity implies that the mass inferred from the 0.8-μm flux alone is an upper limit.

As remarkably distant as Fomalhaut b is from its star, the planet might have formed in situ. The dust belt of Fomalhaut contains three Earth masses of solids in its largest collisional parent bodies. Adding enough gas to bring this material to cosmic composition would imply a minimum primordial disk mass of 1 M_J, comparable to the upper mass limit of Fomalhaut b. Alternatively, the planet might have migrated outward by interacting with its parent disk (*21*) or by gravitationally scattering off another planet in the system and having its eccentricity mildly damped by dynamical friction with surrounding disk material (*22*).

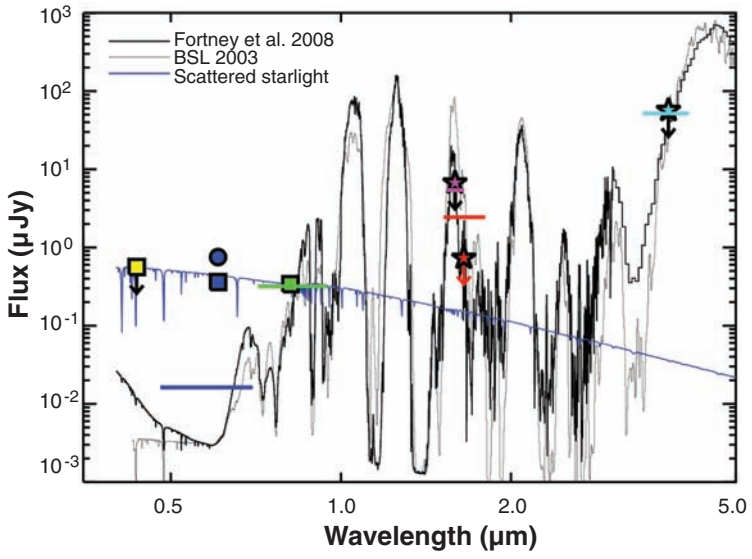

Fig. 3. Photometry on Fomalhaut b shows the F435W 3σ upper limit (yellow square), two F606W measurements (blue square, 2006; blue circle, 2004), the F814W photometry (green square), 3σ upper limits for Keck observations in the CH_4 passband (purple solid star) and in the H band (red solid star), and a 3σ upper limit for Gemini observations at L′ (light blue star). This is a log-log plot. If we first assume that the F606W variability is due to Hα emission and the F814W detection is due to planet thermal emission, we then proceed to fit a planet atmosphere model from Fortney *et al.* (*16*) to the F814W flux. The heavy solid line represents the same planet atmosphere model smoothed to R = 1200 with planet radius 1.2 R_J, gravity 46 m s^{-2}, and T = 400 K (roughly 1 to 3 M_J at 200 My). The horizontal colored lines mark the equivalent broad-band flux found by integrating the model spectrum over the instrumental passband. Other models from Burrows *et al.* [BSL; (*17*)] give a similar spectrum (light solid line), although a factor of 3 to 4 brighter in the CH_4 and H bands. The model predicts that the planet candidate should have been detected with Keck in the H band, although this prediction is only a factor of 3 above our limit. The discrepancy could arise from uncertainties in the model atmosphere (which has never been tested against observation), or from the possibility that the F606W and F814W detections include stellar light reflected from a circumplanetary dust disk or ring system. The solid blue line intersecting the optical data represents light reflected from a circumplanetary disk (with radius 20 R_J and a constant albedo of 0.4) and with stellar properties adopted from (*23*). See table S2 for more information about the HST filters used.

References and Notes

1. D. E. Backman, F. C. Gillett, in *Cool Stars, Stellar Systems and the Sun*, J. L. Linsky, R. E. Stencel, Eds. (Springer-Verlag, Berlin, 1987), pp. 340–350.
2. D. Mouillet, J. D. Larwood, J. C. B. Papaloizou, A. M. Lagrange, *Mon. Not. R. Astron. Soc.* **292**, 896 (1997).
3. M. C. Wyatt *et al.*, *Astrophys. J.* **527**, 918 (1999).
4. One parsec (pc) = 3.09×10^{18} cm.
5. K. Stapelfeldt *et al.*, *Astrophys. J. Suppl. Ser.* **154**, 458 (2004).
6. P. Kalas, J. R. Graham, M. Clampin, *Nature* **435**, 1067 (2005).
7. A. Quillen, *Mon. Not. R. Astron. Soc.* **372**, L14 (2006).
8. D. Barrado y Navascues, *Astron. Astrophys.* **339**, 831 (1998).
9. See supporting material on *Science* Online.
10. C. D. Murray, S. F. Dermott, *Solar System Dynamics* (Cambridge Univ. Press, Cambridge, 1999).
11. B. Paczynski, *Astrophys. J.* **216**, 822 (1977).
12. L. E. Strubbe, E. I. Chiang, *Astrophys. J.* **648**, 652 (2006).
13. J. W. Dohnanyi, *J. Geophys. Res.* **74**, 2531 (1969).
14. J. Wisdom, *Astron. J.* **85**, 1122 (1980).
15. E. Chiang, E. Kite, P. Kalas, J R Graham, M. Clampin, *Astrophys. J.*, in press; http://arxiv.org/abs/0811.1985.
16. J. J. Fortney *et al.*, *Astrophys. J.* **683**, 1104 (2008).
17. A. Burrows, D. Sudarsky, J. I. Lunine, *Astrophys. J.* **596**, 587 (2003).
18. A. J. Burgasser *et al.*, *Astron. J.* **120**, 473 (2000).
19. C. Marois, B. Macintosh, T. Barman, *Astrophys. J.* **654**, L151 (2007).
20. L. Hartmann, R. Hewett, N. Calvet, *Astron. J.* **426**, 669 (1994).
21. D. Veras, P. J. Armitage, *Mon. Not. R. Astron. Soc.* **347**, 613 (2004).
22. E. B. Ford, E. I. Chiang, *Astrophys. J.* **661**, 602 (2007).
23. J. Davis *et al.*, *Astron. Nachr.* **326**, 25 (2005).

24. Supported by HST programs GO-10598 (P.K.) and GO-10539 (K.S. and J.K.), provided by NASA through a grant from the Space Telescope Science Institute (STScI) under NASA contract NAS5-26555; NSF grant AST-0507805 (E.C.); the Michelson Fellowship Program, under contract with JPL, funded by NASA (M.P.F.); and a Berkeley Fellowship (E.S.K.). Work at LLNL was performed under the auspices of the U.S. Department of Energy under contract DE-AC52-07NA27344. We thank the staff at STScI, Keck, and Gemini for supporting our observations.

Supporting Online Material

www.sciencemag.org/cgi/content/full/1166609/DC1
SOM Text
Fig. S1
Tables S1 to S4
References

30 September 2008; accepted 5 November 2008
Published online 13 November 2008;
10.1126/science.1166609
Include this information when citing this paper.

Direct Imaging of Multiple Planets Orbiting the Star HR 8799

Christian Marois,[1,2,3]* Bruce Macintosh,[2] Travis Barman,[4] B. Zuckerman,[5] Inseok Song,[6] Jennifer Patience,[7] David Lafrenière,[8] René Doyon[9]

Direct imaging of exoplanetary systems is a powerful technique that can reveal Jupiter-like planets in wide orbits, can enable detailed characterization of planetary atmospheres, and is a key step toward imaging Earth-like planets. Imaging detections are challenging because of the combined effect of small angular separation and large luminosity contrast between a planet and its host star. High-contrast observations with the Keck and Gemini telescopes have revealed three planets orbiting the star HR 8799, with projected separations of 24, 38, and 68 astronomical units. Multi-epoch data show counter clockwise orbital motion for all three imaged planets. The low luminosity of the companions and the estimated age of the system imply planetary masses between 5 and 13 times that of Jupiter. This system resembles a scaled-up version of the outer portion of our solar system.

During the past decade, various planet detection techniques—precision radial velocities, transits, and microlensing—have been used to detect a diverse population of exoplanets. However, these methods have two limitations. First, the existence of a planet is inferred through its influence on the star about which it orbits; the planet is not directly discerned [photometric signals from some of the closest-in giant planets have been detected by careful analysis of the variations in the integrated brightness of the system as the planet orbits its star (*1*)]. Second, these techniques are limited to small (transits) to moderate (precision radial velocity and microlensing) planet-star separation. The effective sensitivities of the latter two techniques diminish rapidly at semimajor axes beyond about 5 astronomical units (AU). Direct observations allow discovery of planets in wider orbits and allow the spectroscopic and photometric characterization of their complex atmospheres to derive their physical characteristics.

There is indirect evidence for planets in orbits beyond 5 AU from their stars. Some images of dusty debris disks orbiting main-sequence stars (the Vega phenomenon) show spatial structure on a scale of tens to hundreds of astronomical units (*2*). The most likely explanation of such structure is gravitational perturbations by planets with semimajor axes comparable to the radius of the dusty disks and rings [see references in (*3*)].

The only technique currently available to detect planets with semimajor axes greater than about 5 AU in a reasonable amount of time is infrared (IR) imaging of young, nearby stars. The detected near-IR radiation is escaped internal heat energy from the recently formed planets. During

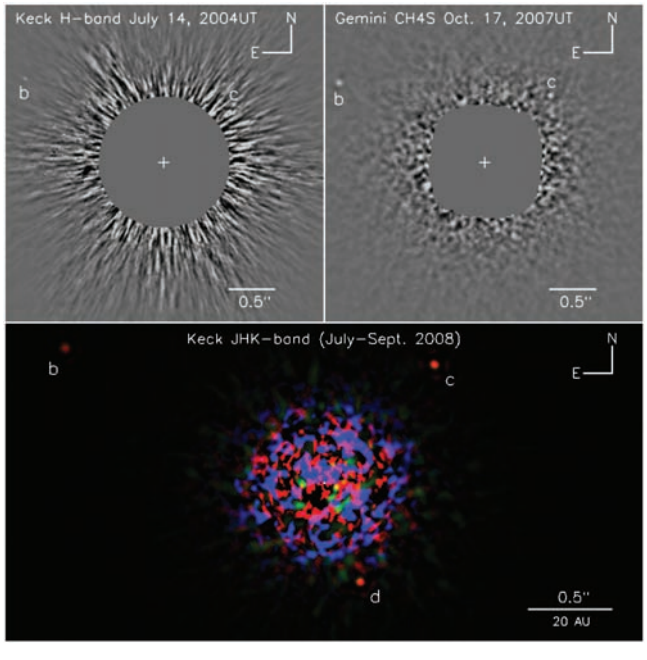

Fig. 1. HR 8799bcd discovery images after the light from the bright host star has been removed by ADI processing. (**Upper left**) A Keck image acquired in July 2004. (**Upper right**) Gemini discovery ADI image acquired in October 2007. Both b and c are detected at the two epochs. (**Bottom**) A color image of the planetary system produced by combining the J-, H-, and Ks-band images obtained at the Keck telescope in July (H) and September (J and Ks) 2008. The inner part of the H-band image has been rotated by 1° to compensate for the orbital motion of d between July and September. The central region is masked out in the upper images but left unmasked in the lower to clearly show the speckle noise level near d.

[1]National Research Council Canada, Herzberg Institute of Astrophysics, 5071 West Saanich Road, Victoria, BC V9E 2E7, Canada. [2]Lawrence Livermore National Laboratory, 7000 East Avenue, Livermore, CA 94550, USA. [3]Astronomy Department, University of California, Berkeley, CA 94720, USA. [4]Lowell Observatory, 1400 West Mars Hill Road, Flagstaff, AZ 86001, USA. [5]Physics and Astronomy Department and Center for Astrobiology, University of California, Los Angeles, CA 90095, USA. [6]University of Georgia, Department of Physics and Astronomy, 240 Physics, Athens, GA 30602, USA. [7]University of Exeter, School of Physics, Stocker Road, Exeter EX4 4QL, UK. [8]Department of Astronomy and Astrophysics, University of Toronto, 50 St. George Street, Toronto, ON M5S 3H4, Canada. [9]Département de Physique and Observatoire du Mont Mégantic, Université de Montréal, C.P. 6128, Succursale Centre-Ville, Montréal, QC H3C 3J7, Canada.

*To whom correspondence should be addressed; E-mail: christian.marois@nrc-cnrc.gc.ca